WARWICK
THE UNIVERSITY OF WARWICK

Original citation:

Rodrigues, N. D. N., Cole-Filipiak, N. C, Horbury, M. D, Staniforth, Michael, Karsili, T. N. V., Peperstraete, Y. and Stavros, Vasilios G.. (2017) Photophysics of the sunscreen ingredient menthyl anthranilate and its precursor methyl anthranilate : a bottom-up approach to photoprotection. Journal of Photochemistry and Photobiology A: Chemistry, 353 . pp. 376-384.

Permanent WRAP URL:

http://wrap.warwick.ac.uk/96191
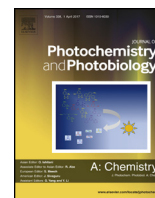
Copyright and reuse:

A note on versions:

The version presented in WRAP is the published version, or, version of record, and may be cited as it appears here.

For more information, please contact the WRAP Team at: wrap@warwick.ac.uk

Photophysics of the sunscreen ingredient menthyl anthranilate and its precursor methyl anthranilate: A bottom-up approach to photoprotection

N.D.N. Rodrigues[a], N.C. Cole-Filipiak[a], M.D. Horbury[a], M. Staniforth[a,b], T.N.V. Karsili[c], Y. Peperstraete[d], V.G. Stavros[a,*]

[a] University of Warwick, Department of Chemistry, Coventry, CV4 7AL, UK
[b] University of Warwick, Department of Physics, Coventry, CV4 7AL, UK
[c] Temple University, Department of Chemistry, Philadelphia, PA 19122, USA
[d] Synchrotron SOLEIL, AILES Beamline, L'Orme des Merisiers, Saint Aubin, BP48, 91192 Gif Sur Yvette Cedex, France

ABSTRACT

The ultrafast excited state dynamics of the sunscreen ingredient menthyl anthranilate (MenA) and its precursor methyl anthranilate (MA) were studied in vacuum (using time-resolved ion yield spectroscopy) and in solution (using transient electronic absorption spectroscopy). MenA and MA both show long-lived dynamics, with the observation of a kinetic isotope effect suggesting that hydrogen motion acts as the rate determining process in the overall decay. Complementary computational studies exploring the intuitive decay pathways of MA revealed a bound S_1 state with a shallow 'up-hill' gradient with respect to proton transfer. From these results, it is suggested that photoexcited population is trapped in this excited state from which luminescence occurs as a prominent decay pathway. This work has shown that the photophysics of MA and MenA – and hence their photoprotection capabilities – are not drastically influenced by aliphatic structure or solvent environment alone. A *bottom-up approach*, such as the one described herein, is essential to understand the combination of factors that afford optimum photoprotection and to develop a new generation of tailor made, efficacious sunscreens.

1. Introduction

The damaging effects of excessive exposure to ultraviolet (UV) radiation to living organisms are well documented in the literature [1–3]. Such damages include erythema [4], a result of excessive skin irradiation with UV-A (400–315 nm) and/or UV-B (315–280 nm) radiation – both of which are directly absorbed by several chromophores in human skin (*e.g.* melanins, acids and kynurenines). UV-A radiation is also linked to production of free radicals and skin aging [5], whilst UV-B radiation can be directly absorbed by DNA and initiate the photochemistry responsible for mutagenic photolesions (*e.g.* cyclobutane pyrimidine dimers) [6]. If repair mechanisms fail to correct these photolesions in DNA, this damage may result in carcinogenesis [7]. While the human skin has its own natural photoprotection mechanisms (provided by melanin pigments), these are often insufficient for continued and excessive sun exposure. Photoprotection products, such as sunscreen lotions, are therefore required in order to provide enhanced protection against UV-induced damage. Since their appearance in the early 20th century [8], sunscreen usage has evolved from simply providing protection against sunburn to being perceived as primary prophylaxis, actively preventing skin aging and skin cancer [9]. Despite attempts to raise awareness of the risks associated with excessive sun exposure and the widespread availability of sunscreen lotions, the incidence of skin cancer has increased in recent years [10]. There is, therefore, an obvious urgency for more effective sunscreens.

An ideal sunscreen molecule should absorb across (and hence provide protection against) the UV-A and UV-B wavelength range of the solar spectrum [11]. One would expect sunscreen molecules to also have the ability to dissipate the absorbed excess energy rapidly – on an ultrafast timescale, *i.e.* femtosecond (10^{-15} s) to picosecond (10^{-12} s) – without detriment to molecular structure. Such detrimental photochemistry may be both intramolecular (fragmentation, isomerisation, *etc.*) and/or intermolecular (chemical reactions with other species in the sunscreen mixture or in the

skin itself) [12–15]. The study of the photodynamics that follow the absorption of UV radiation (photoexcitation) of sunscreen molecules has only recently gained momentum [14–21] and therefore these mechanisms remain poorly understood.

While reports on the ultrafast photodynamics of commonly used sunscreen molecules, such as cinnamates and sinapates [16–18,20], already exist, analogous information is not available for anthranilates such as methyl and menthyl anthranilate (MA and MenA, Fig. 1). MA is a food grade flavour and fragrance additive used in personal care products [22] and is also a precursor to MenA (commercial name *Meradimate*), a sunscreen component approved by the US Food and Drug Administration [23]. In general, the anthranilates are considered to be a photostable (non-degradable upon exposure to UV) class of sunscreens due to the intramolecular hydrogen bonding facilitated by the *ortho* position of the NH_2 group with respect to the ester substituent [24]. Interestingly, however, under anaerobic conditions, a photodegradation mechanism was found to occur for MA upon UV exposure [25]. Under aerobic (more realistic) conditions, an appreciable quantum yield of fluorescence (∼0.376–0.549) was observed in various solvents [26], as well as a 280 μs triplet state lifetime in aqueous solution [22]. Smaller quantum yields for singlet oxygen sensitisation have also been reported for MA [22]. Such radiative and non-radiative processes persist in MenA, which presents large quantum yields for fluorescence (0.64 ± 0.06 in ethanol)[23] and intersystem crossing (0.34 in ethanol at room temperature) [27]. The presence of triplet states in solvated MenA was confirmed by Kikuchi et al. [27] by using a triplet quencher; the lifetime of the triplet state was determined to be 2.36 s [27].

In light of the available literature, it seems that photoexcited MA and MenA dissipate excess energy *via* radiative decay, which is perceivably not ideal in a sunscreen molecule [14]. The radiative decay observed in MA and MenA is at odds with other sunscreen molecules which tend to decay to their ground electronic states *via* non-radiative internal conversion (IC) on an ultrafast timescale [16,19]. It is now well understood that ultrafast IC between electronic states is facilitated by conical intersections (CIs) which arise when certain nuclear motions (*e.g.* isomerisation and bond-stretches) drive distinct electronic states towards degeneracies in configuration space [28]. In related sunscreen molecules, many CI geometries – ranging from *trans-cis* isomerisation to ring deformations, for example – have been identified as likely contributors driving ultrafast IC from the excited to ground state
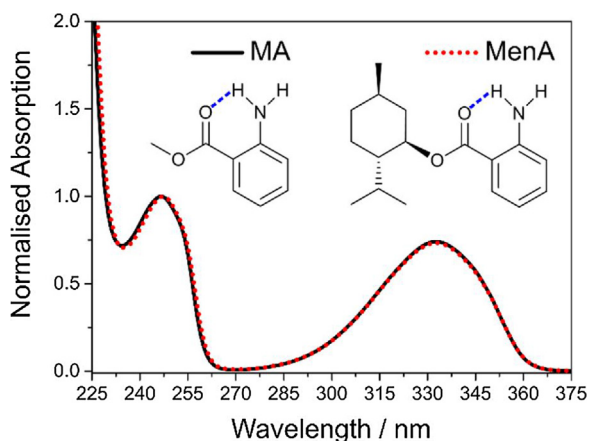
[16,17,29]. For some sunscreen molecules, notably oxybenzone, isomerisation is preceded by an *enol-keto* type hydrogen atom motion; *keto* oxybenzone then isomerises back to ground state *enol* oxybenzone [19]. Such tautomerisation processes typically occur on ultrafast timescales, *i.e.* on much shorter timescales than those probed in the aforementioned MA and MenA studies.

The non-unity luminescence quantum yield of MenA suggests other, non-radiative, photophysical processes are also involved in its relaxation mechanisms. Ultrafast spectroscopy techniques were employed in the present work to identify these ultrafast photophysics taking place in photoexcited MenA and hence further inform on its suitability as a sunscreen ingredient. In keeping with a *bottom-up approach*, by which the effects of increasing molecular complexity are evaluated [14], both MA and MenA were studied. Moreover, spectroscopic techniques were employed both in vacuum and in solution to evaluate the environmental effects on the intrinsic photodynamics of these molecules. Computational studies were also performed to complement the experimental measurements and provide further detail on the topography of the electronic states of the molecules studied. This work highlights the importance of investigative studies targeting the intrinsic molecular and electronic characteristics that provide sunscreen molecules with their photoprotection capabilities.

2. Experimental methods

2.1. Absorption spectra

The UV/Visible absorption spectra of MA (Alfa Aesar, 99%) and MenA (Aldrich, 98%), shown in Fig. 1, were obtained using a PerkinElmer Lambda 850 UV/Vis spectrophotometer. The sample of each molecule was prepared by dissolving MA or MenA in cyclohexane (99%, Fisher Scientific) with a concentration of approximately 10^{-6} M.

2.2. Time-resolved ion yield (TR-IY)

The time-resolved ion yield (TR-IY) set up used in this work has been described previously [30–32] and is therefore only briefly described here, with further details of particular experimental conditions provided where necessary. A commercial femtosecond (fs) Ti:Sapphire oscillator (Spectra-Physics Tsunami) and regenerative amplifier (Spectra-Physics Spitfire XP) were used to produce ∼40 fs laser pulses of ∼3 mJ per pulse centred at 800 nm. The fundamental 800 nm output was subsequently split into three beams, each with ∼1 mJ per pulse. One of these beams was used to pump an optical parametric amplifier (Light Conversion, TOPAS-C) to generate "pump" (λ_{pu}) pulses centred either at 300 nm (4.13 eV), 315 nm (3.94 eV), or 330 nm (3.76 eV). These wavelengths were chosen to sample the UV-A and UV-B regions of the solar spectrum and the broad absorption feature shown in Fig. 1 while maintaining adequate signal to noise ratios. A second laser beam pumped a separate TOPAS-C which was used to generate 260 nm "probe" (λ_{pr}) pulses. The pump and probe pulses were temporally delayed with respect to each other (with a delay time of Δt) by reflecting the pump off a hollow corner gold retroreflector mounted on a motorised delay stage allowing a maximum temporal delay of 1.2 ns.

The two laser beams intersected a molecular beam which was produced by seeding the target molecules, heated to 50 °C (MA) or 90 °C (MenA), into helium (∼3 bar). The gaseous mixture was then expanded into vacuum (∼10^{-7} mbar) using an Even-Lavie pulsed solenoid valve [33]. At the point of intersection, λ_{pu} excited the species in the molecular beam and λ_{pr} ionised any excited (or photodissociated) species. The resulting ions were focused onto a detector, consisting of two microchannel plates (MCPs) coupled to

Fig. 1. UV/Visible absorption spectrum of methyl anthranilate (MA, black solid line) and menthyl anthranilate (MenA, red dotted line) in cyclohexane. The molecular structures of each molecule are also shown, with the intramolecular hydrogen bond indicated with a blue dashed line. (For interpretation of the references to colour in this figure legend, the reader is referred to the web version of this article.)

a phosphor screen, by three ion optics similar to the set up described by Eppink and Parker [34]. The current output from the front of the phosphor screen, gated in ion flight time over the mass channel of each parent ion (MA^+ and $MenA^+$), was measured on a digital oscilloscope (LeCroy LT372 Waverunner) and integrated as a function of Δt in order to produce TR-IY transients. These transients were then modelled using a sum of exponential decays convoluted with a Gaussian instrument response; more details regarding kinetic fits can be found in the Supplementary data, section A (SD.A). Power dependence studies were performed to ensure linear signal intensity *vs.* laser power, *i.e.* that the observed dynamics are due to single-photon photoexcitation. Separate measurements were taken with the polarisations of the pump and probe beams parallel and perpendicular to each other in order to calculate the resulting magic angle equivalent transient [35].

Deuterated MA (d_1-MA and d_2-MA, in which either one or two hydrogens on the amine group were substituted by deuterium atoms, respectively) was produced by stirring MA in d_4-methanol for approximately 72 h under anhydrous N_2. The solvent was then removed under high vacuum (0.5 mbar) in an ice bath ($\sim 0\,°C$); the product was immediately stored under anhydrous N_2 prior to use. The H/D exchange was inferred by the loss/reduction of ^1H NMR signal corresponding to the hydride position due to the formation of two N–D bonds (see SD.B).

2.3. Transient electronic absorption spectroscopy (TEAS)

The TEAS set-up used in the present experiments has been detailed previously [36,37] and is therefore only briefly summarised. TEAS measurements were obtained from separate ~ 1 mM solutions of MA and MenA in both cyclohexane (VWR, >99%) and methanol (Sigma-Aldrich, $\sim 99.6\%$). These solutions were recirculated through a flow cell (Harrick Scientific) consisting of two CaF_2 windows separated by $100\,\mu m$ thick PTFE spacers. Transient absorption spectra (TAS) were obtained by photoexciting the sample using the same TOPAS-C output as for gas-phase experiments, *i.e.* 300 nm, 315 nm and 330 nm pump pulses, with fluences of $1–2\,mJ\,cm^{-2}$ per pulse. The probe pulses consisted of a broadband white light continuum (330–675 nm), generated by focusing a fraction of the third 800 nm fundamental beam into a 2 mm thick CaF_2 window. The relative polarisation between the pump and probe beams was held at magic angle ($54.7°$) by using a $\lambda/2$ waveplate. The time delay between the pump and probe pulses was controlled using a hollow corner gold retroreflector mounted on a motorised translation stage in the probe beam path; maximum $\Delta t = 2$ ns. The setup used in these experiments provides an instrument response function with a full width at half maximum of ~ 80 fs. TAS for each time delay were calculated from the difference in probe pulse intensities passing through sequentially excited and non-excited sample prepared by a mechanical chopper in the pump beam path.

To extract the dynamical information from the TAS, a global fitting sequential model (*e.g.* $A \xrightarrow{\tau_1} B \xrightarrow{\tau_2} C$) was employed using the Glotaran software package [38]. The quality of the fits was evaluated upon inspection of the resulting residuals shown in the SD.C.

3. Computational methods

Using Molpro 2010.1 [39], relaxed potential energy curves (PECs) along the neutral singlet ground state (S_0), the first electronically excited singlet state (S_1), and the cation doublet ground state (D_0^+) were produced using the state-averaged complete active space self-consistent field (SA-CASSCF) [40,41] method coupled to a cc-pVDZ basis set [42]. These PECs were obtained by fixing the H-bonded amino-centred N—H stretch (henceforth N—H_{bound}) at various values (R_{N-Hb}) and allowing the remaining internal degrees of freedom to relax to their respective minima. The active space comprised ten electrons in eight orbitals (10/8), including three π, two n and three π^* valence orbitals. Following separate S_0, S_1 and D_0^+ relaxations across R_{N-Hb}, the energies of the S_0 and S_1 states, the first and second excited triplet states (T_1 and T_2) and the D_0^+ state were computed within each relaxation subset using the complete active space second-order perturbation theory (CASPT2), based on an SA-CASSCF reference wavefunction and a cc-pVDZ basis set. A standard imaginary level shift of 0.5 E_H was used to aid convergence and mitigate the involvement of intruder states.

Two PECs were produced for the S_1 state: one corresponding to the localised excitation (S_1LE) and a second corresponding to charge transfer (S_1CT). The S_1LE PEC describes the case for which charge remains localised on the ring upon photoexcitation ($\pi_{ring} \rightarrow \pi^*_{ring}$). The S_1CT PEC describes instead the case for which, upon photoexcitation, charge is dislocated from the ring π orbital to the carbonyl π^* orbital ($\pi_{ring} \rightarrow \pi^*_{carbonyl}$). Similarly, two PECs associated with the S_0 of MA were calculated: the S_0 PEC was produced by optimising both the geometry and electronic configuration of the S_0 state of MA; the S_0 charge transfer (S_0CT) PEC was produced by optimising the electronic configuration of the S_0 state while keeping the geometry fixed to that of the S_1CT state at each corresponding R_{N-Hb} value.

Following computations along R_{N-Hb}, analogous calculations of the S_0 and S_1 states were undertaken to assess the potential energy topography between $R_{N-Hb} = 1.5\,Å$ to a low-energy S_0/S_1 CI using the CASPT2/cc-pVDZ level of theory. The intermediate geometries between $R_{N-Hb} = 1.5\,Å$ and the S_0/S_1 CI were constructed using a linear interpolation of internal coordinates (LIIC). The CI was optimised using the SA-CASSCF/6-31G(d) level of theory in the Gaussian 09 computational package [43] with a reduced active space of six electrons in six orbitals (6/6).

4. Results

4.1. Time-resolved ion yield (TR-IY)

TR-IY measurements of MA and MenA were taken following photoexcitation at 315 nm and 330 nm. These yielded similar mono-exponential TR-IY transients, shown in Fig. 2, both with decay lifetimes considerably longer than the temporal window of these experiments (>>1.2 ns). In contrast, photoexcitation of MA
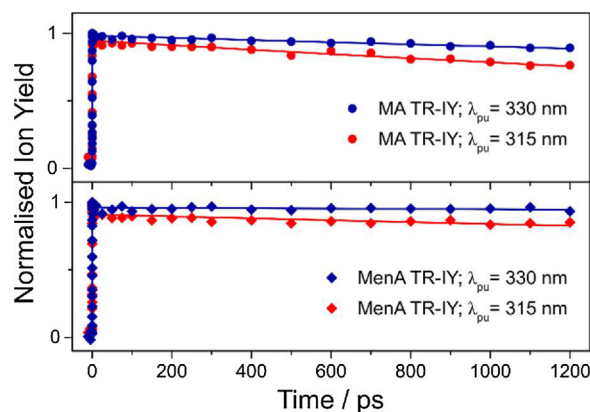

Fig. 2. TR-IY transients resulting from the excitation of MA (top, circles) and MenA (bottom, diamonds) at 315 nm (red) and 330 nm (blue). Solid lines correspond to kinetic fits. (For interpretation of the references to colour in this figure legend, the reader is referred to the web version of this article.)
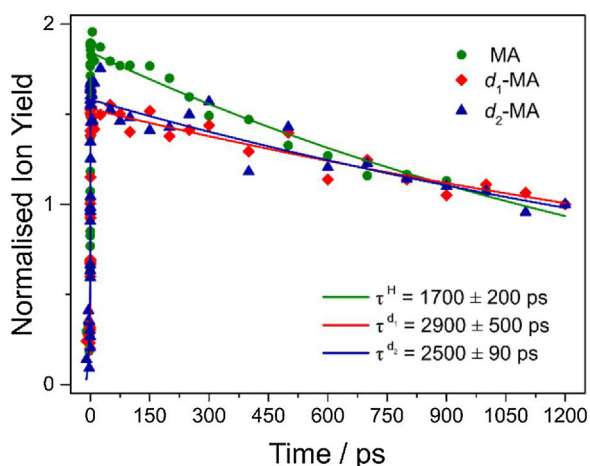
Fig. 3. TR-IY transients resulting from the excitation of MA (green circles), d_1-MA (red diamonds) and d_2-MA (blue triangles) at 300 nm. Data were normalised to their last data point. Solid lines correspond to the kinetic fits used to extract lifetimes. (For interpretation of the references to colour in this figure legend, the reader is referred to the web version of this article.)

at 300 nm results in a faster mono-exponential decay, as shown in green in Fig. 3, with a lifetime $\tau^H \approx 1700 \pm 200$ ps (where the superscript H refers to the hydrogenated MA sample).

Deuterated MA, both d_1-MA and d_2-MA, were also photoexcited with 300 nm and the TR-IY transients are presented in Fig. 3, in red and blue, respectively. It is apparent that deuteration of MA yields slower photodynamics. However, two caveats must be considered in the interpretation of our TR-IY results for deuterated MA. Firstly, the lifetimes extracted from kinetic fits are still outside the temporal window of our experiments and hence the ratio between the lifetimes of MA and d_1/d_2-MA is the focus of our discussion rather than their absolute values. Secondly, we note the low signal-to-noise ratio of our data, particularly in the d_2-MA transient − this is due to a combination of exciting MA at the tail of its absorption (see Fig. 1) and the high levels of D/H exchange experienced during the course of our measurements. Bearing these caveats in mind, we nevertheless quote the extracted lifetimes as follows: $\tau^{d_1} \sim 2900 \pm 500$ ps and $\tau^{d_2} \sim 2500 \pm 90$ ps (where τ^{d_1} and τ^{d_2} refer to the decay time constants of d_1-MA and d_2-MA, respectively). An

average kinetic isotope effect (KIE) of 1.5 ± 0.4 is thus determined from the TR-IY time constants extracted from d_1-MA and d_2-MA.

4.2. Transient electronic absorption spectroscopy (TEAS)

All TAS data, evolution associated difference spectra (EADS) and residuals are shown in the SD.C. A summary of the time constants extracted for both MA and MenA at both photoexcitation wavelengths (315 and 330 nm) can be found in Table 1. For illustrative purposes, the TAS of MA in cyclohexane after photoexcitation with 330 nm are shown in Fig. 4 along with the EADS and associated time constants resulting from the sequential global fit of the returned data.

4.2.1. Cyclohexane

The results of MA in the weakly perturbing solvent, cyclohexane, are presented first as this should be most akin to the environment *in vacuo*. The TAS for both excitation wavelengths (see Fig. 4(a) and SD.C) display similar spectral features and their temporal evolutions are also analogous. As such the results for both wavelengths shall be discussed together. The TAS consist of four features that are apparent after the initial excitation. The negative feature at 385 nm corresponds to stimulated emission (SE) from the initial electronic excited state, which is in good agreement with the measured fluorescence emission wavelength of MA (in ethanol) [12]. Alongside this SE, there is a broad excited state absorption (ESA), again from the initial excited state, spanning

Table 1
Summary of the time constants extracted from the TEAS results for MA and MenA, in cyclohexane (Cy) and methanol (MeOH), at both excitation wavelengths used. *In vacuo* time constants, extracted from our TR-IY measurements, are also presented for comparison.

	MA	
λ_{pu}	315 nm	330 nm
In vacuo	$\tau_1 > 1.2$ ns	$\tau_1 > 1.2$ ns
Cy	$\tau_1 = 10.6 \pm 0.3$ ps	$\tau_1 = 4.6 \pm 0.2$ ps
	$\tau_2 > 2$ ns	$\tau_2 > 2$ ns
	$\tau_3 > 2$ ns	$\tau_3 > 2$ ns
MeOH	$\tau_1 = 3.2 \pm 0.1$ ps	$\tau_1 = 5.9 \pm 0.2$ ps
	$\tau_2 > 2$ ns	$\tau_2 > 2$ ns

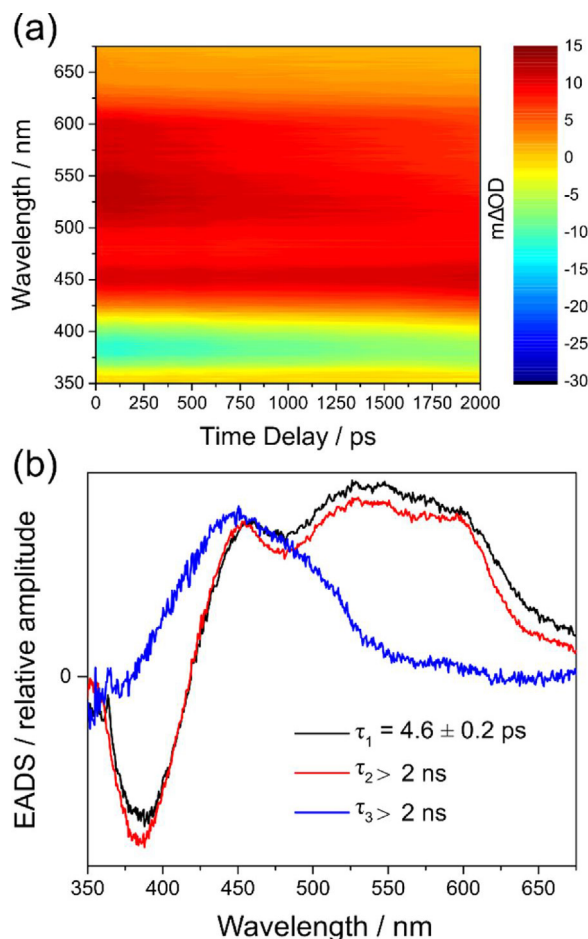|	MenA	
λ_{pu}	315 nm	330 nm
In vacuo	$\tau_1 > 1.2$ ns	$\tau_1 > 1.2$ ns
Cy	$\tau_1 = 1.6 \pm 0.1$ ps	$\tau_1 = 6.6 \pm 0.4$ ps
	$\tau_2 = 1.5 \pm 0.1$ ns	$\tau_2 = 0.6 \pm 0.05$ ns
	$\tau_3 > 2$ ns	$\tau_3 > 2$ ns
MeOH	$\tau_1 = 2.8 \pm 0.1$ ps	$\tau_1 = 5.4 \pm 0.1$ ps
	$\tau_2 > 2$ ns	$\tau_2 > 2$ ns

Fig. 4. (a) TAS spectra for MA in cyclohexane at 330 nm photoexcitation, with (b) respective EADS obtained by fitting with a sequential model. The residuals for this fit, as well as the remaining TEAS data, can be found in the SD.C.
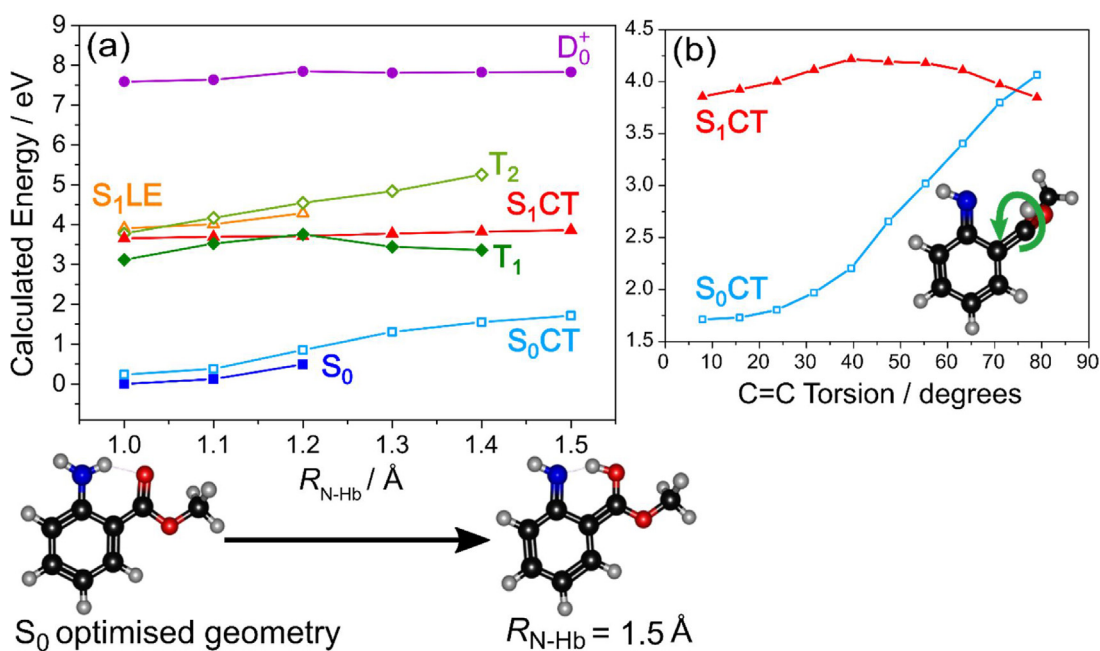
Fig. 5. (a) PECs for various electronic states of MA along the R_{N-Hb} coordinate, for which a hydrogen migrates from the amine group towards the neighbouring carbonyl oxygen. Below the plot, the S_0 optimised geometry (*keto*, left) and the proton transfer geometry, *i.e.* at R_{N-Hb} = 1.5 Å (*enol*, right) are also shown. Presented here are the ground state (S_0, blue squares) and the charge transfer ground state (S_0CT, hollow light blue squares), the locally excited first singlet state (S_1LE, hollow orange triangles) and first excited singlet state, which has charge transfer character (S_1CT, red triangles), the first and second triplet states (T_1, green diamonds, and T_2, hollow light green diamonds, respectively) and the first cationic surface (D_0^+, purple circles). (b) PECs for the S_0CT and S_1CT states along the coordinate corresponding to the twisting motion around the C—C bond connecting the phenyl ring and the ester substituent. This motion is illustrated by the inset on the lower right corner. (For interpretation of the references to colour in this figure legend, the reader is referred to the web version of this article.)

420 nm to 675 nm, with three distinct peaks at 455 nm, 525 nm and 580 nm. The dynamics of MA in cyclohexane, from black to red in Fig. 4(b), can be described simply as a narrowing of the excited state spectrum (*e.g.* the decrease in intensity around 625 nm) and a slight blue shift of all features (most easily seen in the negative feature at ~380 nm) within τ_1, with excited state population then persisting beyond 2 ns (τ_2). A third time component is also necessary to successfully fit the TAS; this is shown in Fig. 4(b) as the blue EADS and is associated with the decay time constant $\tau_3 > 2$ ns. Equivalent spectra for MenA are very similar: features are observed within the same wavelength ranges and qualitatively the same time dependent behaviour is observed, albeit with some differences in extracted time constants, as summarised in Table 1.

4.2.2. Methanol

TEAS measurements were also carried out in methanol, a more perturbing solvent than cyclohexane given its polarity. The TAS for MA and MenA at both excitation wavelengths also display similar features in methanol (see SD.C). The time constants obtained for MA and MenA in methanol are summarised in Table 1. In all cases (both molecules and pump wavelengths), the TAS consist of three main features which appear upon photoexcitation. A SE feature from the first excited electronic state is observed at 400 nm, which is in good agreement with the reported fluorescence emission

Table 2
Calculated vertical excitation energies for some of the singlet and triplet excited states of MA.

Electronic state of MA	Vertical excitation energy (eV)
$T_1(\pi\pi^*)$	3.12
$S_1CT(\pi\pi^*)$	3.66
$T_2(\pi\pi^*)$	3.76
$S_1(\pi\pi^*)$	3.91

wavelength of MenA in ethanol. [27] The broad ESA in methanol extends from 430 nm to 675 nm, with prominent peaks at 450 nm and 600 nm. Similar to the observation in cyclohexane, the dynamics of both MA and MenA in methanol can be described as a narrowing and spectral shift of the observed features, as discussed above. However, τ_3 is not required in methanol to properly fit the data.

4.3. Computational studies

The relaxed potential energy curves (PECs) for several excited states of MA were calculated, namely: the ground state (locally excited, S_0LE, and charge transfer, S_0CT), the first electronically excited singlet state (locally excited, S_1LE, and charge transfer, S_1CT), the first and second excited triplet states (T_1 and T_2) and the cation doublet ground state (D_0^+). These PECs are presented in Fig. 5 and a summary of the vertical excitation energies calculated for the S_1, S_1CT, T_1 and T_2 states of MA is given in Table 2.

The PECs in Fig. 5(a) were calculated as a function of length of the intramolecular N—H bond, from R_{N-Hb} = 1 Å (*keto* tautomer) to R_{N-Hb} = 1.5 Å (*enol* tautomer). The S_0 optimised geometry, corresponding to the *keto* tautomer, is also displayed in Fig. 5(a), along with the proton transfer (*enol*) geometry. These PECs reveal a lack of driving force for complete proton transfer on both the S_0 and S_1CT states, evidenced by their increase in molecular potential energy along the R_{N-Hb} coordinate (1.5 eV rise for S_0 and 0.21 eV for S_1CT). The PECs for MA presented in Fig. 5(a) also suggest a strong degeneracy of the S_1CT and T_1 states (near R_{N-Hb} = 1.2 Å).

PECs for the S_0CT and S_1CT states of MA from the geometries at R_{N-Hb} = 1.5 Å and then along the C=C twisting motion coordinate (*i.e.* rotation of the ester group with respect to the phenyl ring) were also produced and are displayed in Fig. 5(b). While the upper limit barrier to this twisting motion in MA was calculated to be 0.4 eV above the S_1CT energy at R_{N-Hb} = 1.5 Å, this motion was also

found to lead to a S_1/S_0 CI. The calculated geometry at this CI is also presented in Fig. 5(b).

Additional computational results, including *i)* PECs along the $S_1LE \rightarrow S_1CT$ coordinate; *ii)* PECs along the N—H and O—Me bond dissociation coordinates; *iii)* the optimised geometry at the S_1/S_0 CI; and *iv)* the Cartesian coordinates for the optimised S_0, S_1 and S_1/S_0 CI geometries, can be found in SD.F.

5. Discussion

In broad terms, all the dynamics observed for both MA and MenA at various pump energies and various environments are long-lived and strikingly similar. Particularly in vacuum, the results for both molecules are remarkably similar; the TR-IY transients, albeit qualitatively faster at higher pump energy, all show lifetimes > 1.2 ns. In solution, there are other differences brought on by solvent-solute interaction. The behaviour of MA and MenA in cyclohexane is described by three time constants, rather than the two required to fit the data in methanol (*vide infra* for further discussion). Nevertheless, regardless of environment or pump wavelength, both MA and MenA display similar photodynamics, always with a long-lived excited state which is observed to persist for at least 1–2 ns. Moreover, the UV/Visible spectra for MA and MenA (Fig. 1) are, once again, very similar, indicating that the additional menthyl unit in MenA does not perturb the low energy electronic states of the system, as could be expected given the non-perturbative character of the menthyl unit (*i.e.* since the menthyl unit does not provide any extra conjugation or otherwise significantly alter the electronic density of MA). Therefore, the dynamics of MA and MenA will be discussed jointly throughout this section, with attention being drawn to any differences between them as appropriate.

For MA, the first band in the UV/Visible spectrum, ranging from 360 nm to 290 nm, is assigned to the $S_1(\pi\pi^*)$ state based on the calculated vertical excitation energies (Table 2). Hence, excitation within the $330 \geq \lambda \geq 300$ nm pump wavelength range (3.76–4.13 eV) used in these experiments is likely to exclusively populate the S_1 state. In the gas-phase, photoexcitation at either 315 nm or 330 nm yields a mono-exponential TR-IY transient that does not recover to the baseline within the timescale observable in these experiments, *i.e.* 1.2 ns. When MA is photoexcited at 300 nm, however, there is a marked difference in the resulting transient, in that a single lifetime of $\tau^H \approx 1700 \pm 200$ ps is now extracted (with some certainty, since the half-life is within our temporal probe window). The long-lived photodynamics observed suggest that any fast relaxation pathways from the S_1 state are negligible and that photoexcited population is trapped in the S_1 state for at least a nanosecond.

Considering the amine group of MA, one of the intuitive ultrafast decay pathways to consider would be N—H$_{free}$ (non-intramolecularly bound) bond dissociation, as has been observed in aniline [44]. Experimentally, however, resonantly probing H-atoms (with a 243 nm probe) yields no obvious H$^+$ signal attributable to the formation of single-photon induced N—H$_{free}$ bond fission along a dissociative excited state (see SD.E) [44]. Moreover, computational studies reveal a large barrier to N—H$_{free}$ bond fission relative to the S_1 minimum, further suggesting that this is not a viable relaxation pathway for MA (see SD.F). Similarly, computational studies predict a bound first excited state along the O—Me fission coordinate; this relaxation pathway is thus also ruled out. Prefulvenic pathways are also unlikely to be responsible for the photodynamics observed in our experiments since they are usually accessed at energies much higher than our photoexcitation range [44,45].

In other structurally similar systems [46–48], such as salicylic acid [49,50], an initially locally excited $^1\pi\pi^*$ state may couple to a low-lying charge transfer (CT) state upon photoexcitation, which can mediate proton transfer along an intramolecular hydrogen bond. This type of excited state intramolecular proton transfer (ESIPT) is well reported in the literature [51–54] and has been observed in the sunscreen molecule oxybenzone [19]. While salicylic acid undergoes a complete hydrogen transfer [49,50], anthranilic acid (the carboxylic acid variant of MA) has been reported to instead undergo excited state hydrogen atom *dislocation*, with one of the amine hydrogens migrating towards the carbonyl oxygen (akin to an incomplete *keto-enol* tautomerisation) [55]. Parallel photoelectron spectroscopy measurements on MA and MenA (see SD.G) did not yield the expected distinctive features for a complete proton transfer mechanism, that is, there were no discrete electron kinetic energy features that could be assigned to the *keto* and/or *enol* forms of MA [56]. Hence, it is plausible to conclude that, similar to the case of anthranilic acid, hydrogen atom dislocation along the intramolecular hydrogen bond takes place in photoexcited MA, instead of complete proton transfer.

The possibility of hydrogen atom dislocation occurring in MA was evaluated experimentally by obtaining TR-IY transients for MA, d_1-MA and d_2-MA photoexcited at 300 nm. From the time constants extracted, an average kinetic isotope effect (KIE) of 1.5 ± 0.4 (approximately $\sqrt{2}$) was determined, suggesting that non-tunnelling hydrogen atom motion is indeed involved in the dynamics observed for MA. Further evidence supporting a hydrogen dislocation mechanism in MA is provided by the PECs displayed in Fig. 5(a), which reveal a lack of driving force for complete proton transfer on these states, as previously discussed. However, excitation in the $330 \geq \lambda \geq 300$ nm pump wavelength range (3.76–4.13 eV) is likely to provide sufficient energy for the relatively shallow S_1CT state to be sampled, and hence for the aforementioned hydrogen atom dislocation to take place.

Given the experimentally determined KIE for MA and upon analysis of the PECs in Fig. 5, we propose that, after photoexcitation with $330 \geq \lambda \geq 300$ nm, the excited state population of MA relaxes from the locally excited ($\pi_{ring} \rightarrow \pi^*_{ring}$) S_1 state to the more stable CT ($\pi_{ring} \rightarrow \pi^*_{carbonyl}$) S_1 state (see SD.F), where it is then trapped in a relatively shallow well. The lack of direct evidence for this $S_1LE \rightarrow S_1CT$ transfer in our gas-phase experiments (*i.e.* no corresponding decay time constant), could be due to this process happening on a timescale faster than that measurable in these experiments. Such charge migration phenomena have been observed to occur on sub-femtosecond timescales (see, for example, reference [57]), which would make it impossible to resolve with our experimental setup.

In other systems, including other sunscreen molecules, proton transfer is followed by a twisting motion which eventually leads to a low-energy S_1/S_0 CI. [19,46–49] The analogous motion in MA would be around the C=C bond connecting the phenyl ring and the ester substituent, as demonstrated in Fig. 5(b). However, the barrier to this motion in MA is much higher when compared to that of similar molecules (*e.g.* 0.4 eV in MA *vs.* 0.1 eV in salicylic acid). [49] This barrier may explain the marked difference in behaviour for MA photoexcited at 315 nm or 330 nm ($\tau >> 1.2$ ns, see Fig. 2) when compared to photoexcitation at 300 nm ($\tau^H \approx 1700 \pm 200$ ps, see Fig. 3), since 300 nm (4.1 eV) would provide just enough energy to surmount the barrier, thus accelerating the overall decay of MA (when compared to photoexcitation at 315 nm or 330 nm). The existence of a barrier *en route* to the S_1/S_0 CI is also consistent with the proposed trapping of the excited state population in the S_1CT state. Despite the impact that a barriered process may have on the photodynamics of MA, the fact that a KIE is observed in our studies (while N—H$_{free}$ bond fission is not) shows that it is hydrogen motion along the intramolecular hydrogen bond that acts as the 'rate determining step' in the excited state relaxation of MA at 300 nm. Presumably, it would be the coupling of the N—H—O

motion to other vibrational modes or electronic states that ultimately facilitates the final decay of MA.

With excited state population trapped in the S_1CT state, and with no direct evidence for any CIs or any dissociative relaxation pathways that can be accessed on an ultrafast timescale from the S_1CT state, photoexcited MA would be expected to radiatively decay to its ground state. As mentioned in the introduction, there is extensive reporting of luminescence in both MA and MenA in the literature. Significant fluorescence quantum yields have been reported for both molecules, [23,26,27] with the observed emission wavelength being approximately 400 nm ($\sim$3.1 eV). We note here that this emission wavelength of 400 nm matches best with the calculated energy difference between the S_1CT and the S_0CT states in the region closer to the vertical excitation region of the PEC. Hence, while the excited state population may sample the entirety of the S_1CT state, transition to the ground state appears to be more likely at short N—H_{bound} bond distances. This apparent emission dependence on geometry, namely on N—H_{bound} bond distances, further highlights the significance of the hydrogen motion in the photodynamics of MA, as discussed earlier.

Finally, despite the requirements of El Sayed's rule not being met for $S_1CT(\pi\pi^*) \rightarrow T_1(\pi\pi^*)$, the strong degeneracy of singlet and triplet states in MA (near $R_{N-Hb} = 1.2$ Å, see Fig. 5(a)), could facilitate intersystem crossing (ISC) and, consequently, phosphorescence. While there is no direct evidence for ISC in the gas-phase experiments reported here, previous studies in solution have found photoexcitation of MA to result in an excited triplet state with a lifetime of 280 μs. [22] In MenA, the reported triplet state lifetime is 2.36 ± 0.01 s, with a phosphorescence quantum yield of $\Phi_P = 0.092 \pm 0.009$. [27] The insensitivity of our gas-phase experiments to ISC ($S_1CT \rightarrow T_1$) may be due to the very similar surfaces of their respective PECs (see Fig. 5(a)). The transition between these states ($S_1CT \rightarrow T_1$) may be difficult to distinguish in these experiments due to very similar ionisation cross sections, the effect likely being accentuated by the shallow character of the PEC of the first cationic state, D_0^+. Therefore, it is reasonable to assume that, while ISC occurs in both MA and MenA, it may be convoluted and hence indistinguishable in our gas-phase experiments. It is also possible that ISC occurs outside the temporal window of these experiments (as our TEAS results suggest, *vide infra*).

The results from our experiments in solution reveal a similar decay mechanism for both MA and MenA, with evidence for luminescence. Immediately obvious is the agreement between the wavelength of the SE component observed in our experiments and the previously measured emission wavelength of both MA and MenA, both at $\sim$400 nm, [23,26,27] which provides evidence for fluorescence. Evidence for the existence of triplet states in both MA and MenA − and, hence, phosphorescence − can be drawn from a close analysis of the EADS and extracted decay time constants, as is now discussed. The sequential model fit of the obtained TAS in cyclohexane yields $\tau_1 \sim 2$–11 ps (depending on specific molecule and pump wavelength). This time constant is assigned to vibrational energy transfer (VET), which includes both intramolecular vibrational redistribution (IVR) and intermolecular energy transfer (IET). Since IET is a process by which vibrational cooling is achieved by energy transfer to the solvent, this is a process that cannot occur in the gas-phase. The variation in τ_1 can then be understood in terms of varying degrees of solvent-solute interactions which will have an effect on the rate of IET. [58] The TAS for both molecules in cyclohexane (at either pump wavelength) require two more time constants for a successful fit. For MA, τ_2 is simply assigned to the decay of the relaxed S_1 state, akin to our observations in vacuum; τ_3 is assigned to the decay of the triplet state of MA, since the EADS corresponding to τ_3 are spectrally very similar to the triplet state transient absorption spectrum of MenA which Kikuchi et al. obtained. [27]

There are two main differences for the analogous time constants extracted for MenA: *i*) the EADS associated with τ_3 do not resemble the aforementioned measurements by Kikuchi et al., but instead seem to retain some of the spectral features that are assigned to the long-lived S_1 state (see SD.D) and *ii*) τ_2 varies between $\sim$0.6–1.5 ns (*c.f.* > 2 ns for MA). As discussed in more detail in the SD.D, subtracting the normalised τ_3 EADS from those of τ_2 yields a spectrum that is indeed similar to measurements which Kikuchi et al. carried out (in ethanol). Hence, we propose that the spectral differences between our MenA results in cyclohexane and the previously reported triplet state transient absorption are due to extensive convolution of the processes associated to τ_2 and the appearance of a triplet state. The shortening of τ_2 may therefore not be a reflection of a faster decay of the S_1 state, but rather a result of our sequential model not being able to deconvolute the processes associated with τ_2 and τ_3. Indeed, the fact that the long-lived component observed for MenA in cyclohexane (τ_3 > 2 ns) contains spectral features similar to the EADS corresponding to τ_2 suggests that the S_1 state is still populated at 2 ns (the limit of the probe window of these experiments).

To conclude the discussion of our results in cyclohexane, we note that, contrary to the observation in vacuum, photoexcitation of MA at 300 nm does not drastically accelerate its decay (see SD.C). It is likely that IET in solution facilitates faster relaxation to the S_1 minimum, from which the barrier to twisting motion can no longer be overcome (see above). Moreover, we note that EADS for MA in cyclohexane at 300 nm are similar to those of MenA (at other excitation wavelengths), which supports the theory that the spectral/temporal discrepancies discussed earlier are due to the sequential model used to fit these data, rather than any chemical or physical differences between MA or MenA.

In methanol, on the other hand, only two time constants are necessary to fit the TAS of each molecule; there is no evidence for triplet states in this solvent for either MA or MenA. However, triplet states were previously observed in MenA in ethanol [27], hence it is highly likely that triplet states are formed in methanol for both MA and MenA outside the temporal window of our TEAS experiments. Assuming dislocation of the intramolecularly bound hydrogen atom is as relevant in solution as we proposed in the discussion of our results in vacuum, and hence considering that hydrogen motion facilitates ISC, it would not be surprising that a polar protic solvent would affect the observed behaviour of MA and MenA.

In summary, regardless of pump wavelength (315 nm *vs.* 330 nm, and 300 nm for MA), environment (vacuum *vs.* solution), and/or solvent polarity (cyclohexane *vs.* methanol), the photodynamics of MA and MenA can essentially be described as a slow decay corresponding to long-lived excited states which will likely luminesce. The differences in molecular structure between MA and MenA do not change the observed photodynamics (as is the observation for other sunscreen molecules and their precursors) [16,29] to such an extent that would justify the use of either molecule as a sunscreen, as far as photochemical and/or photophysical factors are concerned. The lack of a drastic solvent effect on the photodynamics of MA or MenA, on the other hand, is in stark contrast with observations for other sunscreens, which reinforces the importance of a fundamental understanding of sunscreen photophysics [16,29].

It transpires from our experiments that the intramolecular hydrogen bond present in MA and MenA affords them a first singlet excited state in which the intramolecularly bound hydrogen is dislocated from the amine towards the carbonyl oxygen, with the proton transfer never being complete. Thus, the intramolecular hydrogen bond of the anthranilates is responsible for the observed long-lived excited state. The enhanced stability of their excited

states means that photoexcitation of MA/MenA with UV-A and UV-B radiation − the wavelength range of interest in a sunscreen context − provides insufficient energy for excited state population to access any CIs that would facilitate ultrafast relaxation. This, in turn, is a non-ideal scenario for sunscreen molecules since the long lifetime of any excited (potentially reactive) states may increase the chance for undesirable intra- or intermolecular chemical reactions. Nevertheless, MenA is used in the sunscreen industry – albeit scarcely – which raises the question: what is the fate of the excess energy in MenA after absorption of UV radiation by a sunscreen lotion? To address this question, our studies on isolated molecules will need to be expanded towards complex mixtures of sunscreen molecules, solvents, stabilisers, etc. Of particular relevance are the recent studies by Matsumoto et al. which have reported diffusion-controlled (highly efficient) triplet–triplet energy transfer processes from MenA to other sunscreen molecules (octocrylene and octyl methoxycinnamate) [59]. This work by Matsumoto et al. highlights the importance of identifying and understanding the fates of excess energy in a sunscreen context. In addition, further research into the photophysics of sunscreen molecules is necessary to identify the molecular/electronic features that allow for ideal photoprotective characteristics.

6. Conclusion

The similarity of the results for MA and MenA in vacuum are in accordance with observations for other sunscreen molecules, which have similar photodynamics to those of their precursors [29]. Nevertheless, molecular structure alterations – particularly those of a more perturbative nature – will of course have an impact in a molecule's photodynamics as has been shown for other systems [20]. External environment factors, such as solvents, also tend to have a great impact in the observed photodynamics [16,29]. However, interestingly, this is not the case for the systems under study in this work. We have shown that, photophysically speaking, both MA and MenA behave as non-ideal sunscreens independently of external environment.

Designing sunscreen molecules for optimised photoprotection can only be achieved once the molecular characteristics which provide photoprotective capabilities are identified. To identify these photoprotection-affording characteristics, it is necessary to consider the effects of molecular structure on the electronic energy topography of the chromophore. This should culminate in a comprehensive understanding not only of light absorption, but also of the ensuing photodynamics in these molecules. In the cases explored in this work, we suggest that the intramolecular hydrogen bond stabilises the excited states of MA and MenA, preventing any molecular fragmentation from occurring but ultimately hindering effective dissipation of potentially harmful excess energy. The S_1/S_0 CI along a twisting motion coordinate, common for other ESIPT molecules, is inaccessible in these anthranilates (upon photoexcitation with UV-A/B). Our work therefore highlights two aspects of the anthranilates that may be interrogated in order to drive faster excited state decays in MA and MenA: i) alterations to the intramolecular hydrogen bond, e.g. changing the amine group by a different substituent, change its ring position or eliminate it altogether; and ii) changing the substituent functional groups in an attempt to lower the barrier to the twisting motion. In addition, these studies on isolated molecules will need to be expanded towards more realistic environments in the sunscreen context, i.e. complex mixtures of sunscreen molecules, solvents, stabilisers, etc. Work is currently underway to investigate these effects in our laboratory.

Appendix A. Supplementary data

Supplementary data associated with this article can be found, in the online version, at https://doi.org/10.1016/j.jphotochem.2017.11.042.

Any remaining data, supporting information and clarifications can be found in the supplementary data document published alongside this article. The Supplementary material provided consists of: **A.** Kinetic Fits; **B.** MA and d_2-MA ^{1}H NMR; **C.** Remaining TEAS spectra for MA and MenA with respective EADs and fit residuals; **D.** Triplet state appearance in MenA in cyclohexane; **E.** Velocity Map Imaging (VMI) of H-atoms. **F.** Additional results from computational studies. **G.** Photoelectron Spectroscopy.

References

[1] F.R. de Gruijl, Eur. J. Cancer 35 (1999) 2003–2009, doi:http://dx.doi.org/10.1016/s0959-8049(99)00283-x.
[2] F.R. de Gruijl, Methods Enzymol. 319 (2000) 359–366, doi:http://dx.doi.org/10.1016/s0076-6879(00)19035-4.
[3] R.P. Sinha, D.P. Häder, Photochem. Photobiol. Sci. 1 (2002) 225–236, doi:http://dx.doi.org/10.1039/b201230h.
[4] M. Brenner, V.J. Hearing, Photochem. Photobiol. 84 (2008) 539–549, doi:http://dx.doi.org/10.1111/j.1751-1097.2007.00226.x.
[5] J.L. McCullough, K.M. Kelly, Ann. N. Y. Acad. Sci. 1067 (2006) 323–331, doi:http://dx.doi.org/10.1196/annals.1354.044.
[6] D.E. Brash, Photochem. Photobiol. 91 (2015) 15–26, doi:http://dx.doi.org/10.1111/php.12377.
[7] F.R. De Gruijl, H. Rebel, Photochem. Photobiol. 84 (2008) 382–387, doi:http://dx.doi.org/10.1111/j.1751-1097.2007.00275.x.
[8] J.L.M. Hawk, European Handbook of Dermatological Treatments, Springer, Berlin Heidelberg, 2015, pp. 1519–1528, doi:http://dx.doi.org/10.1007/978-3-662-45139-7_149.
[9] A.S. Farberg, A.M. Glazer, A.C. Rigel, R. White, D.S. Rigel, J. Am. Med. Assoc.: Dermatol. 153 (2017) 99–101, doi:http://dx.doi.org/10.1001/jamadermatol.2016.3698.
[10] N.A. Shaath, Principles and Practice of Photoprotection, Springer International Publishing, 2016, pp. 143–157, doi:http://dx.doi.org/10.1007/978-3-319-29382-0_9.
[11] U. Osterwalder, B. Herzog, Photochem. Photobiol. Sci. 9 (2010) 470–481, doi:http://dx.doi.org/10.1039/b9pp00178f.
[12] A.E. Jones, Doctor of Philosophy, Durham University, 2000.
[13] R. Krishnan, N. Kollias, C.A. Elmets, B. Choi, H. Zeng, T.M. Nordlund, R.S. Malek, B.J. Wong, J.F.R. Ilgner, K.W. Gregory, et al., SPIE Proc. 6842 (2008) 6842081–6842088, doi:http://dx.doi.org/10.1117/12.758693.
[14] N.D. Rodrigues, M. Staniforth, V.G. Stavros, Proc.e R. Soc. A 472 (2016) 20160677, doi:http://dx.doi.org/10.1098/rspa.2016.0677.
[15] L.A. Baker, V.G. Stavros, Sci. Prog. 99 (2016) 282–311, doi:http://dx.doi.org/10.3184/003685016x14684992086383.
[16] E.M. Tan, M. Hilbers, W.J. Buma, J. Phys. Chem. Lett. 5 (2014) 2464–2468, doi:http://dx.doi.org/10.1021/jz501140b.
[17] Y. Miyazaki, K. Yamamoto, J. Aoki, T. Ikeda, Y. Inokuchi, M. Ehara, T. Ebata, J. Chem. Phys. 141 (2014) 244313, doi:http://dx.doi.org/10.1063/1.4904268.
[18] J.C. Dean, R. Kusaka, P.S. Walsh, F. Allais, T.S. Zwier, J. Amer. Chem. Soc. 136 (2014) 14780–14795, doi:http://dx.doi.org/10.1021/ja5059026.
[19] L.A. Baker, M.D. Horbury, S.E. Greenough, P.M. Coulter, T.N. Karsili, G.M. Roberts, A.J. Orr-Ewing, M.N. Ashfold, V.G. Stavros, J. Phys. Chem. Lett. 6 (2015) 1363–1368, doi:http://dx.doi.org/10.1021/acs.jpclett.5b00417.
[20] N.D. Rodrigues, M. Staniforth, J.D. Young, Y. Peperstraete, N.C. Cole-Filipiak, J.R. Gord, P.S. Walsh, D.M. Hewett, T.S. Zwier, V.G. Stavros, Faraday Discuss. 194 (2016) 709–729, doi:http://dx.doi.org/10.1039/c6fd00079g.

[21] M.D. Horbury, L.A. Baker, N.D.N. Rodrigues, W.-D. Quan, V.G. Stavros, Chem. Phys. Lett. 673 (2017) 62–67, doi:http://dx.doi.org/10.1016/j.cplett.2017.02.004.

[22] C. Gambetta, J. Natera, W.A. Massad, N.A. García, J. Photochem. Photobiol. A: Chem. 269 (2013) 27–33, doi:http://dx.doi.org/10.1016/j.jphotochem.2013.06.013.

[23] A. Beeby, A.E. Jones, Photochem. Photobiol. 72 (2000) 10–15, doi:http://dx.doi.org/10.1562/0031-8655(2000)072<0010:tppoma>2.0.co;2.

[24] N.J. Lowe, N.A. Shaath, M.A. Pathak, Sunscreens: Development, Evaluation, and Regulatory Aspects, Marcel Dekker Inc, New York, 1997.

[25] L.C. Eugeny Aronov, Pestic. Sci. 47 (1996) 355–362, doi:http://dx.doi.org/10.1002/(SICI)1096-9063(199608)47:4<355:AID-PS429>3.0.CO;2-3.

[26] W.H. Melhuish, J. Phys. Chem. 65 (1961) 229–235, doi:http://dx.doi.org/10.1021/j100820a009.

[27] A. Kikuchi, K. Shibata, R. Kumasaka, M. Yagi, Photochem. Photobiol. Sci. 12 (2013) 246–253, doi:http://dx.doi.org/10.1039/c2pp25190f.

[28] G.A. Worth, L.S. Cederbaum, Ann. Rev. Physi. Chem. 55 (2004) 127–158, doi:http://dx.doi.org/10.1146/annurev.physchem.55.091602.094335.

[29] Y. Peperstraete, M. Staniforth, L.A. Baker, N.D. Rodrigues, N.C. Cole-Filipiak, W.D. Quan, V.G. Stavros, Phys. Chem. Chem. Phys. 18 (2016) 28140–28149, doi:http://dx.doi.org/10.1039/c6cp05205c.

[30] A. Iqbal, M.S. Cheung, M.G. Nix, V.G. Stavros, J. Phys. Chem. A 113 (2009) 8157–8163, doi:http://dx.doi.org/10.1021/jp9031223.

[31] K.L. Wells, G. Perriam, V.G. Stavros, J. Chem. Phys. 130 (2009) 074308, doi:http://dx.doi.org/10.1063/1.3072763.

[32] M. Staniforth, J.D. Young, D.R. Cole, T.N. Karsili, M.N. Ashfold, V.G. Stavros, J. Phys. Chem. A 118 (2014) 10909–10918, doi:http://dx.doi.org/10.1021/jp508919s.

[33] U. Even, J. Jortner, D. Noy, N. Lavie, C. Cossart-Magos, J. Chem. Phys. 112 (2000) 8068, doi:http://dx.doi.org/10.1063/1.481405.

[34] A.T.J.B. Eppink, D.H. Parker, Rev. Sci. Instrum. 68 (1997) 3477–3484, doi:http://dx.doi.org/10.1063/1.1148310.

[35] D. Imanbaew, M.F. Gelin, C. Riehn, Struct. Dyn. 3 (2016) 043211, doi:http://dx.doi.org/10.1063/1.4953367.

[36] S.E. Greenough, M.D. Horbury, J.O. Thompson, G.M. Roberts, T.N. Karsili, B. Marchetti, D. Townsend, V.G. Stavros, Phys. Chem. Chem. Phys. 16 (2014) 16187–16195, doi:http://dx.doi.org/10.1039/c4cp02424a.

[37] S.E. Greenough, G.M. Roberts, N.A. Smith, M.D. Horbury, R.G. McKinlay, J.M. Zurek, M.J. Paterson, P.J. Sadler, V.G. Stavros, Phys. Chem. Chem. Phys. 16 (2014) 19141–19155, doi:http://dx.doi.org/10.1039/c4cp02359e.

[38] J.J. Snellenburg, S.P. Laptenok, R. Seger, K.M. Mullen, I.H.M.V. Stokkum, J. Statistical Softw. 49 (2012), doi:http://dx.doi.org/10.18637/jss.v049.i03.

[39] H.J. Werner, P.J. Knowles, G. Knizia, F.R. Manby, M. Schütz, Wiley Interdisciplinary Rev.: Comput. Mol. Sci. 2 (2012) 242–253, doi:http://dx.doi.org/10.1002/wcms.82.

[40] H.J. Werner, W. Meyer, J. Chem. Phys. 74 (1981) 5794–5801, doi:http://dx.doi.org/10.1063/1.440892.

[41] P.G. Szalay, T. Muller, G. Gidofalvi, H. Lischka, R. Shepard, Chem. Rev. 112 (2012) 108–181, doi:http://dx.doi.org/10.1021/cr200137a.

[42] T.H. Dunning, J. Chem. Phys. 90 (1989) 1007–1023, doi:http://dx.doi.org/10.1063/1.456153.

[43] M.J. Frisch, G.W. Trucks, H.B. Schlegel, G.E. Scuseria, M.A. Robb, J.R. Cheeseman, G. Scalmani, V. Barone, G.A. Petersson, H. Nakatsuji, et al., Gaussian 09 (2016).

[44] G.M. Roberts, C.A. Williams, J.D. Young, S. Ullrich, M.J. Paterson, V.G. Stavros, J. Am. Chem. Soc. 134 (2012) 12578–12589, doi:http://dx.doi.org/10.1021/ja3029729.

[45] B. Marchetti, T.N. Karsili, M.N. Ashfold, W. Domcke, Phys. Chem. Chem. Phys. 18 (2016) 20007–20027, doi:http://dx.doi.org/10.1039/c6cp00165c.

[46] T.N. Karsili, B. Marchetti, M.N. Ashfold, W. Domcke, J. Phys. Chem. A 118 (2014) 11999–12010, doi:http://dx.doi.org/10.1021/jp507282d.

[47] D. Tuna, N. Doslic, M. Malis, A.L. Sobolewski, W. Domcke, J. Phys. Chem. B 119 (2015) 2112–2124, doi:http://dx.doi.org/10.1021/jp501782v.

[48] R. Omidyan, M. Iravani, J. Phys. Chem. A 120 (2016) 1012–1019, doi:http://dx.doi.org/10.1021/acs.jpca.5b12122.

[49] A.L. Sobolewski, W. Domcke, Phys. Chem. Chem. Phys. 8 (2006) 3410–3417, doi:http://dx.doi.org/10.1039/b604610j.

[50] T. Raeker, B. Hartke, J. Phys. Chem. A 121 (2017) 5967–5977, doi:http://dx.doi.org/10.1021/acs.jpca.7b03261.

[51] J. Zhao, S. Ji, Y. Chen, H. Guo, P. Yang, Phys. Chem. Chem. Phys. 14 (2012) 8803–8817, doi:http://dx.doi.org/10.1039/c2cp23144a.

[52] S.J. Lim, J. Seo, S.Y. Park, J. Am. Chem. Soc. 128 (2006) 14542–14547, doi:http://dx.doi.org/10.1021/ja0637604.

[53] J.E. Kwon, S.Y. Park, Adv. Mater. 23 (2011) 3615–3642, doi:http://dx.doi.org/10.1002/adma.201102046.

[54] F.S. Rodembusch, F.P. Leusin, L.F. Campo, V. Stefani, J. Lumin. 126 (2007) 728–734, doi:http://dx.doi.org/10.1016/j.jlumin.2006.11.007.

[55] C.A. Southern, D.H. Levy, G.M. Florio, A. Longarte, T.S. Zwier, J. Phys. Chem. A 107 (2003) 4032–4040, doi:http://dx.doi.org/10.1021/jp027041x.

[56] A. Stolow, Annu. Rev. Phys. Chem. 54 (2003) 89–119, doi:http://dx.doi.org/10.1146/annurev.physchem.54.011002.103809.

[57] F. Calegari, A. Trabattoni, A. Palacios, D. Ayuso, M.C. Castrovilli, J.B. Greenwood, P. Decleva, F. Martín, M. Nisoli, J. Phys. B: At. Mol. Opt. Phys. 49 (2016) 142001, doi:http://dx.doi.org/10.1088/0953-4075/49/14/142001.

[58] H.J. Bakker, J. Chem. Phys. 98 (1993) 8496–8506, doi:http://dx.doi.org/10.1063/1.464508.

[59] S. Matsumoto, R. Kumasaka, M. Yagi, A. Kikuchi, J. Photochem. Photobiol. A: Chem. 346 (2017) 396–400, doi:http://dx.doi.org/10.1016/j.jphotochem.2017.06.020.